Geodesy and Geodynamics xxx (2017) 1–7

Contents lists available at ScienceDirect

Geodesy and Geodynamics

journal homepages: www.keaipublishing.com/en/journals/geog;
http://www.jgg09.com/jweb_ddcl_en/EN/volumn/home.shtml

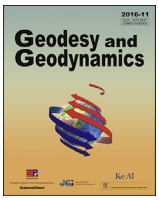

Influence of ocean tidal loading on InSAR offshore areas deformation monitoring

Mengfei Lei, Qijie Wang*, Xiaoli Liu, Bing Xu, Hongqiang Zhang

School of Geosciences and Info-Physics, Central South University, Changsha 410083, China

ARTICLE INFO

Article history:
Received 29 June 2016
Accepted 12 September 2016
Available online xxx

Keywords:
Ocean tidal loading
InSAR
Improved regional model
Present model
IGS station

ABSTRACT

The ocean tide can cause the redistribution of the seawater mass, resulting in earth's surface deformation, namely ocean tidal loading (OTL). OTL vertical displacement may reach several centimeters, especially in coastal areas, so its effect in the field of high precision geodesy must be considered. This study concentrates on the influences of OTL on InSAR deformation measurements. We improve the osu.chinasea.2010 regional model and then compare the improved regional model with other regional models. It turns out that the improved regional model can achieve higher precision. Then we use it to replace the offshore part of the global model to generate the present model. We find that the displacement observed by the present model is 2–3 mm larger than that of other models on some sites. Finally, the present model is used to correct the deformation observed by InSAR of Shanghai and Los Angeles. A comparison between the displacements of IGS station with the corrected data shows that the OTL correction can improve the accuracy of InSAR deformation results by about 20%.

1. Introduction

Ocean Tidal Loading (OTL) is the elastic response of the earth to the redistribution of water mass from the ocean tides [1]. It causes periodic displacements to ground stations, which vary with the station locations. In coastal areas, OTL displacements can be several centimeters [2], seriously affecting the accuracy of geodetic surveying. Therefore, OTL displacements should be considered in high-precision geodetic surveying.

As OTL effects become increasingly prominent, many global ocean tidal models and regional models have been put forward, laying a solid foundation for more precise studies. Using hydrodynamical interpolation methods, Schwiderski established the first relatively accurate global ocean tide model, the SCHW80, in 1980 with the data of more than 2000 gauge stations [3]. After that, series FES94.1 to FES2004, series GOT00 to GOT4.8, series TPXO.2 to TPXO7.2, NAO99JB, and osu.chinasea.2010 [4] were proposed gradually. These global ocean tide models are precise and similar in calculating OTL displacements of the seafloor. However, they can't provide accurate observation in offshore areas, where the seafloor relieves are complicated. Penna et al. found that for International GNSS Service (IGS) sites, the root mean square (RMS) error is about 3 mm in the vertical direction when using different tidal models, but for some coastal areas (such as the Weddell sea and Antarctic Ross ice shelf) the RMS can be up to 8 mm [5]. Therefore, it is important to improve the accuracy of ocean tide models in coastal areas.

Interferometric Synthetic Aperture Radar (InSAR) is a new technology for earth observation from the space and has been widely used in monitoring, seismic displacement, volcanic eruption, glacial drift, land subsidence and landslide [6–11]. However, OTL's impact was often ignored in processing the InSAR data. Some studies have shown that the OTL displacement in coastal areas can be several centimeters, especially in the vertical direction [12]. And the temporal InSAR can achieve millimeter-level precision, when the long time series InSAR data are available. Hence, the effect of OTL should be considered, especially in coastal areas. And the wide use of ScanSAR also requires the consideration of the deformation

* *Corresponding author.* Fax: +86 731 88830573.
E-mail address: qjwang@csu.edu.cn (Q. Wang).

Peer review under responsibility of Institute of Seismology, China Earthquake Administration.

Production and Hosting by Elsevier on behalf of KeAi

http://dx.doi.org/10.1016/j.geog.2016.09.004

caused by OTL in InSAR deformation monitoring. At present, the OTL correction has been used in GPS, Very Long Baseline Interferometry (VLBI) and other high precision space geodesy technology. DiCaprio Christopher J. and Simons Mark have proven that OTL can cause deformation up to millimeters or even centimeters near coastal regions [13]. Rignot considered OTL correction in the research of glacial drifts using InSAR, and gained a good result finally [14]. However, there is very few researches about OTL displacement correction in coastal areas deformation monitoring by InSAR.

In this study, we firstly improve the osu.chinasea.2010 regional model by assimilating data from 60 offshore gauge stations in China, and then compare the results obtained by the improved regional model with those of the tpxo7.2-atlas ocean tide model. Afterwards, we calculate the OTL displacements of some stations in China using the improved regional model. Finally, we correct the deformation obtained by InSAR in Shanghai and Los Angeles, and then compare the results with the displacements of IGS station.

2. Theory of OTL and OTL displacement correction

The tidal loading is computed by the Green's function of ocean loading [15]. The OTL displacements $L(\varphi,\lambda,t)$ is given by

$$L(\varphi,\lambda,t)=\iint_S \rho R^2 H(\varphi',\lambda',t)G(\theta)\sin\varphi' \mathrm{d}\varphi' \mathrm{d}\lambda' \tag{1}$$

where ρ is the ocean water density, φ is the observation of the calculation point, λ is the longitude of the observation point, φ' is the colatitude of the load point, λ' is the longitude of the load point, $H(\varphi',\lambda',t)$ is the tidal height at (φ',λ'), $G(\theta)$ is the Green's function of mass loading, θ is the angular distance between the observation point and the load point, R is the earth radius [16].

We mainly discuss the displacement in the vertical (UP), north-south (NS) and east-west (EW) directions. The OTL displacement can be written as

$$\begin{aligned} L(\varphi,\lambda) &= [L_{\mathrm{UP}}(\varphi,\lambda)\ \ L_{\mathrm{NS}}(\varphi,\lambda)\ \ L_{\mathrm{EW}}(\varphi,\lambda)]^{\mathrm{T}} \\ G(\theta,A) &= [U(\theta)\ \ V(\theta)\cos A\ \ V(\theta)\sin A]^{\mathrm{T}} \end{aligned} \tag{2}$$

where $V(\theta)$ and $U(\theta)$ are the mass loading Green's functions in the horizontal and vertical directions, which can be written as [17]:

$$\begin{aligned} U(\theta) &= \frac{Rh'_\infty}{2M\sin\frac{\theta}{2}} + \frac{R}{M}\sum_{n=0}^{N}(h'_n - h'_\infty)P(\cos\theta) \\ V(\theta) &= \frac{Rl'_\infty\cos\frac{\theta}{2}\left(1+2\sin\frac{\theta}{2}\right)}{2M\sin\frac{\theta}{2}\left(1+\sin\frac{\theta}{2}\right)} + \frac{R}{M}\sum_{n=0}^{N}(nl'_n - l'_\infty)\frac{1}{n}\frac{\partial P_n(\cos\theta)}{\partial\theta} \end{aligned} \tag{3}$$

Due to the complex submarine topography in offshore areas, observations obtained by global ocean models (such as TPXO7.2-ATLAS model) are low in precision, especially in the Western Pacific regions. Therefore, we employ regional model in this study, which can be expressed as:

$$\begin{aligned} L(\varphi,\lambda,t) = &\iint_{S-\Omega}\rho R^2 H(\varphi',\lambda',t)G(\theta)\sin\varphi' \mathrm{d}\varphi' \mathrm{d}\lambda' \\ &+ \iint_{\Omega}\rho R^2 H_\Omega(\varphi',\lambda',t)G_\Omega(\theta)\sin\varphi' \mathrm{d}\varphi' \mathrm{d}\lambda \end{aligned} \tag{4}$$

where Ω is the area, $H_\Omega(\varphi',\lambda',t)$ the tidal height and $G_\Omega(\theta)$ the mass loading Green's function of the interest offshore areas.

There are many non-tectonic deformations in InSAR researches, such as, solid earth tides, pole tide, seasonal and non-seasonal non-tidal loading. Blewitt found that the wavelengths of solid earth tides and pole tide have an order of magnitude greater than ocean tide loading [18]. What's more, we can eliminate solid earth tides and pole tide loading by introducing an additional phase. However, atmospheric loading is similar to ocean loading effects, and atmospheric loading displacements can be centimeter-level [19]. Therefore, we also consider the atmospheric loading effects in this study. As the deformation obtained by InSAR is in line of sight (LOS), but the atmospheric loading and the OTL displacement is positive in the vertical upward direction. The InSAR OTL correction can be expressed in the following formula.

$$LOS_{\mathrm{IOT}} = LOS_{\mathrm{INSAR}} - (V_{\mathrm{AT}} + V_{\mathrm{OTL}})/\cos\alpha \tag{5}$$

where LOS_{IOT} is the deformation with OTL correction in the LOS direction, LOS_{INSAR} is the deformation without OTL correction, V_{OTL} is the OTL displacement, V_{AT} is the atmospheric loading, α is the squint angle of SAR satellite. V_{AT} can be expressed by the following formula.

$$V_{\mathrm{AT}}(\varphi',\lambda',t) = \iint_S G(\delta)P(\varphi,\lambda,t)\mathrm{d}s \tag{6}$$

where $G(\delta)$ is the atmospheric loading Green's function, $P(\varphi,\lambda,t)$ is the average atmospheric pressure of integral area element ds that related to colatitudes φ and longitude λ, (φ',λ') are the colatitude and longitude of observation point, δ is the angular distance between the observation point and the load point [20].

3. Chinese offshore regional ocean tide model

3.1. Improved osu.chinasea.2010 model

The osu.chinasea.2010 model, proposed by Y.Erofeeva and G.Egbert, is a regional ocean tide model covering the range from 1°N to 42°N and from 98°E to 129°E [21], with a resolution of $2' \times 2'$. It is suitable for the research of ocean tide in China. To describe the tidal characteristics more accurately, we used the blending method to assimilate tidal gauge data from 60 offshore gauge stations (55 gauge stations in the South China Sea and 5 gauge stations in the Bohai Sea) in China, and thus has got the improved osu.chinasea.2010 model. The blending method was presented in Matsumoto (2000) [22], it predicted tidal height by a weighted sum of the model prediction and the observed tidal gauge height. The improved osu.chinasea.2010 model (hereafter referred to as the improved regional model) is shown in Fig. 1. We compare the osu.chinasea.2010, the improved regional model and the TPXO7.2-ATLAS model in terms of the root sum square (RSS) and root mean square (RMS),

$$RMS = \sqrt{\frac{1}{2N}\sum_{i=1}^{N}|H_{\mathrm{Si}} - H_{\mathrm{Oi}}|^2} \tag{7}$$

where N is the number of stations, H_{Si} is the amplitude of station i calculated by these models, H_{Oi} is the observed value of station i.

We only calculate tidal components M_2 and K_1, because their amplitudes are greater than other components. The results are listed in Table 1.

Clearly, the improved regional model has far smaller RMS and RSS than those of the tpxo7.2-atlas model, suggesting its accuracy is much higher than that of tpxo7.2-atlas in offshore areas, especially in the South China Sea. Because of assimilating method and fewer gauge data, it is difficult to have a great improvement upon the old model. The RMS and RSS of improved regional model are both slightly smaller than osu.chinasea.2010 except the RMS of $K1$ in the

Please cite this article in press as: M. Lei, et al., Influence of ocean tidal loading on InSAR offshore areas deformation monitoring, Geodesy and Geodynamics (2017), http://dx.doi.org/10.1016/j.geog.2016.09.004

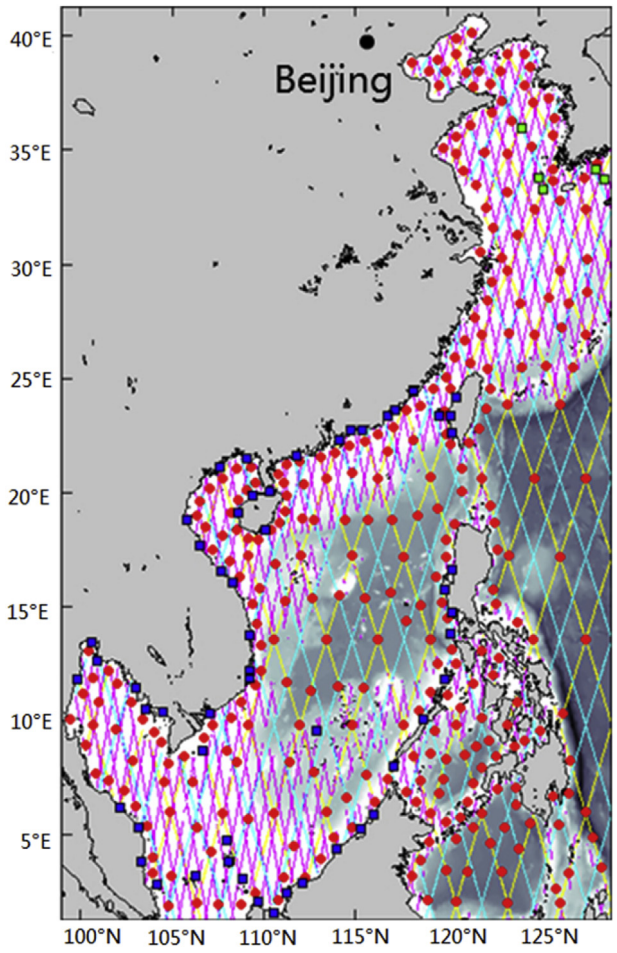

Fig. 1. Improved osu.chinasea.2010 model. The altimeter data are represented by red dots, the gauge stations in South China Sea emerge as solid blue squares, the gauge stations in the Bohai Sea are presented by green dots. Modified from Stammer [23].

Table 1
Accuracy analysis of the tide models in China's offshore areas.

Ocean tide models	RMS (the South China Sea)		RMS (the Bohai Sea)		RSS
	M_2	K_1	M_2	K_1	
tpxo7.2-atlas	11.73	6.96	7.65	1.30	15.69
osu.chinasea.2010	4.16	1.63	4.77	0.97	6.61
Improved regional model	4.09	1.60	4.71	0.98	6.51

Bohai Sea. Compared with the osu.chinasea.2010 model, it doesn't achieve great improvement, which may be caused by the insufficient assimilation data, but it is improved after all.

3.2. Analyses of OTL displacement

We use the improved regional model to analyze the amplitude and phase lag of diurnal tides (K1, O1, P1, Q1) and semi-diurnal tides (M2, S2, N2, K2) and found that *M*2 and *K*1 are more typical, as their amplitudes are greater than other tidal components. We only study the displacements of *M*2 and *K*1 tidal constituents. We replace the offshore part of the global model with the improved regional model to generate an present model, with which we calculate the displacements of *M*2 and *K*1 at 17 reference stations (see Fig. 2) evenly distributed in China. The results are then compared with those of FES2004, TPXO7.2-ATLAS and NAO99JB models. By using Gutenberg-BullenA earth model, we calculated the loading love numbers and obtain loading Green's functions, then we calculated amplitude (amp) and phase lag of *M*2 and *K*1 through loading Green's functions. The results are shown in Tables 2 and 3. The phase lag uses the Greenwich phase as a benchmark, and the negative is on the delay angle.

As is shown in Tables 2 and 3, based on the results of the present model, the OTL effect on the inland is much smaller than that on the coastal areas, and it gradually decreases east-westward. In terms of *M*2, its influence on the Xiamen station ranks the biggest (8.896 mm), followed by the Shanghai station (7.592 mm). Inland western stations such as Urumqi (0.358 mm) and Lhasa (0.525 mm) expose to little influence. Displacements in Qiongzhong (3.577 mm) and Yongshu Reef (4.674 mm), are relatively small, indicating that the effect of *M*2 tidal constituent is smaller in the South China Sea. With regard to *K*1, the maximum amplitude happens in the Fiery Cross Reef (16.727 mm), which is also consistent with the distribution features of the diurnal tides in the South China Sea. Generally, displacement of *K*1 is bigger than that of *M*2 at sites in the Central and Western China except for Kunming and Lhasa. In the South China Sea, the *K*1 tidal constituent displacement is several times higher than that of *M*2, such as Fiery Cross Reef (16.727 *vs.* 4.674)and Qiongzhong sites (6.541 *vs.* 3.577). But their effects on the displacement in coastal regions are similar. To conclude, the effect of diurnal tides is greater than semi-diurnal tides in central and western regions, while the opposite situation arises in the Taiwan Strait and the East China Sea Region. But both tides exert great influence on precise positioning and small deformation detection.

The results of TPXO7.2-ATLAS and FES2004 are similar. But the present model shows a relatively large difference from the NAO99Jb model, especially at Shanghai, Xiamen, Qiongzhong and Yongshu Reef sites. This is mainly due to the fact that the NAO99Jb regional model (latitude rang: 20°N–65°N) was built for observing Japanese areas without considering the effects of the South China Sea. In addition, the OTL displacement of these five sites (Shanghai, Xiamen, Qiongzhong, Guangzhou, Yongshu Reef) calculated by the present model is 2–3 mm larger than the results of other models. But for the rest sites, the difference is less than 1 mm. It proves that the present model can increase the accuracy of OTL displacement in coastal areas.

4. Influence of OTL on coastal areas deformation monitoring using InSAR

We use the observations of IGS stations to verify InSAR results after the OTL correction. Besides the InSAR data of Shanghai, we also choose the InSAR data of Los Angeles, where IGS sites are relatively denser. The OTL displacement in Los Angeles is calculated by the present model. Figs. 3 and 4 are the cotidal charts of Shanghai and Los Angeles, respectively. *M*2 and *K*1 possess the biggest amplitudes among the seven main tidal constituents. It can be seen from Fig. 3 that the distribution characteristics of *M*2 are more complicated than those of *K*1. Fig. 4 informs us that *M*2 and *K*1 are relatively steady in offshore areas on the west coast, with their amplitude being 0.6 m and 0.4 m respectively and no abnormal amplitudes. Due to the complex changes of *M*2 tidal constituent, we apply it to research the influence of OTL on deformation monitoring.

Using the SAR data obtained by ERS1/2, spanning from 1996 to 1999 for Shanghai and from 2005 to 2010 for Los Angeles, we got the deformation in these two places, shown in Figs. 5(a) and 6(a). The maximum distance from land to the coastline in Shanghai and Los Angeles is about 95 km and 107 km, respectively. In the SAR

Please cite this article in press as: M. Lei, et al., Influence of ocean tidal loading on InSAR offshore areas deformation monitoring, Geodesy and Geodynamics (2017), http://dx.doi.org/10.1016/j.geog.2016.09.004

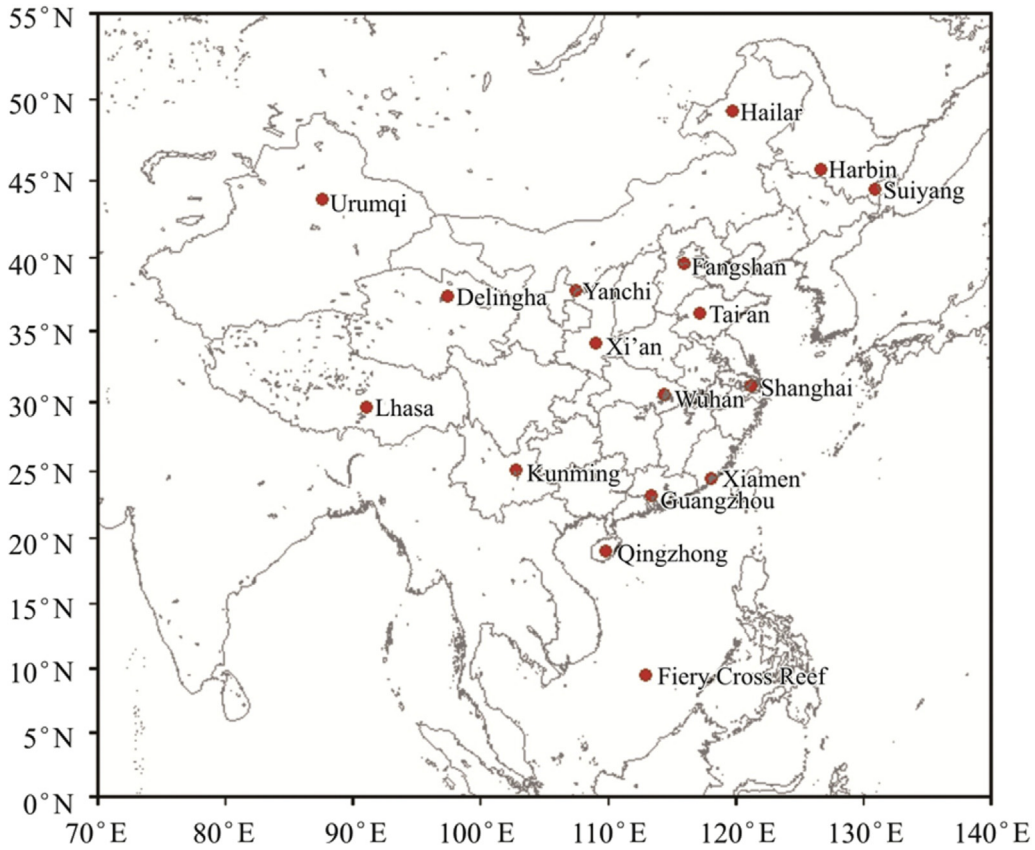

Fig. 2. Distribution of some crustal movement observation stations in China.

Table 2
M2 tidal constituent displacement of different models in the vertical direction.

Sites	Present model		NAO99Jb		TPXO7.2-ATLAS		FES2004	
	Amp. (mm)	Phase lag (degree)	Amp. (mm)	Phase lag (degree)	Amp. (mm)	Phase lag (degree)	Amp. (mm)	Phase lag (degree)
Fangshan	2.145	−109.3	2.138	−105.9	2.060	−110.7	2.012	−117.9
Suiyang	2.548	−74.3	2.532	−88.4	2.418	−74.2	2.435	−74.8
Hailar	1.693	−87.8	1.626	−92.6	1.479	−87.8	1.480	−92.6
Taian	2.758	−123.6	2.624	−120.3	2.556	−124.2	2.547	−131.2
Wuhan	3.235	−144.5	3.038	−139.6	3.269	−145.2	3.240	−146.0
Guangzhou	4.408	−168.7	3.600	−166.7	3.900	−169.4	4.000	−169.8
Yanchi	1.556	−123.7	1.530	−119.1	1.569	−123.6	1.573	−129.9
Xi'an	2.080	−131.8	1.862	−129.5	2.028	−132.8	2.075	−136.2
Kunming	1.889	−155.9	1.733	−153.4	1.867	−155.4	1.964	−160.8
Delingha	0.624	−130.0	0.558	−122.2	0.623	−130.5	0.654	−139.6
Lhasa	0.525	124.8	0.468	120.2	0.502	127.5	0.490	133.9
Urumqi	0.358	6.4	0.299	3.6	0.307	7.3	0.262	10.6
Harbin	2.185	−86.2	2.162	−93.8	2.155	−86.3	2.053	−89.1
Shanghai	7.592	152.5	5.218	135.1	5.695	152.9	6.096	157.0
Xiamen	8.896	109.7	6.714	130.7	6.867	104.8	6.573	107.8
Qiongzhong	3.577	174.5	2.828	175.7	2.825	175.2	2.613	171.9
Fiery Cross Reef	4.674	146.7	3.802	145.2	3.750	146.9	3.761	150.7

images, points P (121°7′44.1″E, 31°21′54.4″N) (Fig. 5) and Q (118°00′14″W, 34°1′22″ N) (Fig. 6) show good coherence and have node formation, so we choose them as reference points.

As we can see from the Fig. 5(a), the contour of OTL is dense in the coastal areas with the maximum value close to 16 mm, and the OTL displacement gradually decreases from coastal to inland areas. This tendency is quite outstanding in the Chongming Island. Also, there is obvious effect of atmospheric loading in Shanghai (the maximum value is 9 mm), which gradually decreases from high latitudes to low latitudes. Three areas (a, b and c) with remarkable subsidence (maximum 126.8 mm from 1996 to 1999). While some areas are experiencing uplift, with the maximum being 57.4 mm.

In Fig. 6(a), the OTL contour of Los Angeles shows the same characteristics with that of Shanghai. Atmospheric loading effect is very small, but with more uniform distribution. Except for three obvious subsidence areas (maximum 100.8 mm from 2005 to 2010), the whole ground underwent uplift, and the maximum uplift is 126.8 mm.

As the deformation obtained by InSAR is relative displacement, while the OTL and atmospheric loading displacements are absolute

Please cite this article in press as: M. Lei, et al., Influence of ocean tidal loading on InSAR offshore areas deformation monitoring, Geodesy and Geodynamics (2017), http://dx.doi.org/10.1016/j.geog.2016.09.004

Table 3
−*K*1 tidal constituent displacement of different models in the vertical direction.

Sites	Present model		NAO99Jb		TPXO7.2-ATLAS		FES2004	
	Amp. (mm)	Phase lag (degree)	Amp. (mm)	Phase lag (degree)	Amp. (mm)	Phase lag (degree)	Amp. (mm)	Phase lag (degree)
Fangshan	3.454	113.3	3.493	112.5	3.353	112.4	3.357	113.1
Suiyang	2.318	131.4	2.419	128.0	2.980	131.6	2.944	131.3
Hailar	3.908	127.7	3.858	122.7	3.556	127.3	3.566	127.5
Taian	3.581	105.3	3.619	104.8	3.461	105.2	3.486	105.0
Wuhan	3.296	85.8	3.283	85.3	3.056	87.1	3.091	85.5
Guangzhou	4.761	31.3	4.355	32.8	4.355	31.9	4.379	30.8
Yanchi	2.267	100.7	2.311	100.9	2.281	101.1	2.259	100.5
Xi'an	2.381	91.6	2.396	91.2	2.394	92.4	2.389	91.3
Kunming	1.583	40.8	1.513	38.2	1.560	42.7	1.590	39.6
Delingha	1.340	100.6	1.327	100.4	1.341	100.8	1.332	100.2
Lhasa	0.287	78.9	0.213	78.5	0.310	85.1	0.293	77.1
Urumqi	1.170	121.1	1.157	120.7	1.157	121.1	1.168	121.0
Harbin	4.407	128.9	4.803	125.1	4.424	129.0	4.416	128.8
Shanghai	6.398	98.8	5.959	101.4	5.665	98.0	5.647	98.7
Xiamen	6.414	51.6	6.325	56.6	6.065	51.3	6.103	50.2
Qiongzhong	6.541	−8.0	4.006	−10.1	4.193	−8.5	4.172	−8.4
Fiery Cross Reef	16.727	−5.0	15.534	−5.3	16.274	−5.5	16.348	−5.0

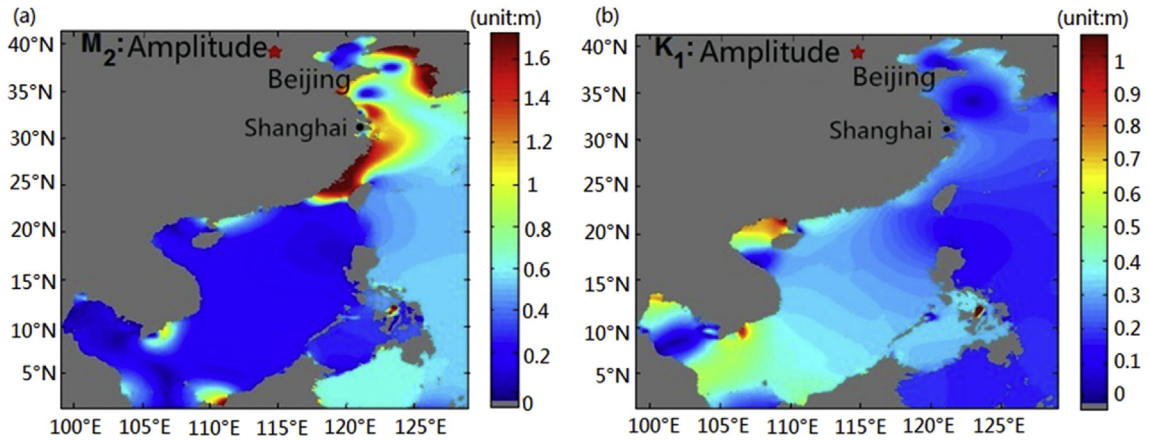

Fig. 3. Distribution of (a) *M*2, (b) *K*1 in Chinese offshore.

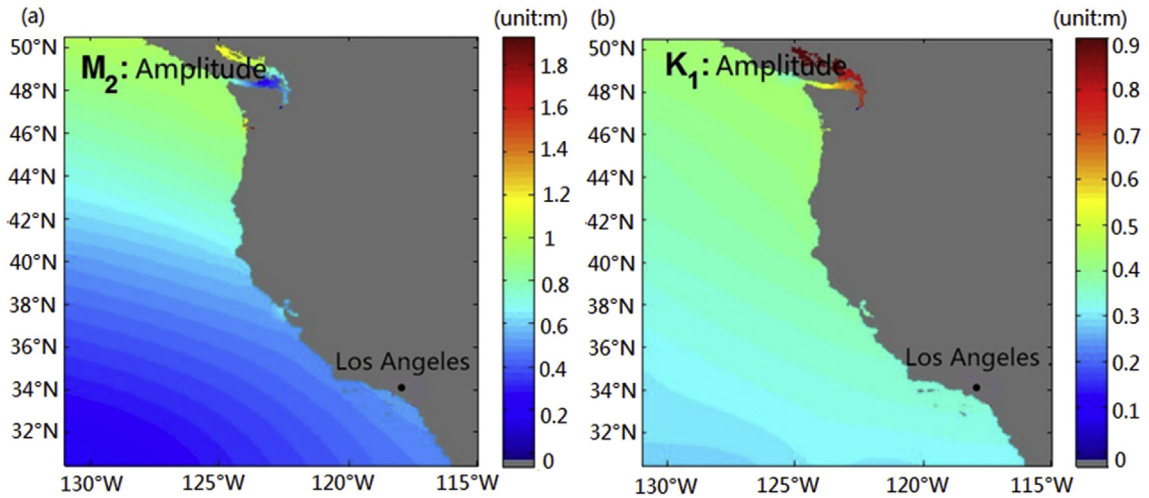

Fig. 4. Distribution of (a) M2, (b) K1 in the west coast of America.

displacement, we need convert the absolute displacement to the relative displacement in respect to point P and Q, which will then be corrected by Formula (5). And the results are shown in Figs. 5(b) and 6(b). As we can see maximum subsidence in Fig. 5(b) is bigger than Fig. 5(a) (131.1 mm *vs.* 126.8 mm), but the maximum uplift is smaller (50.7 mm *vs.* 57.4 mm). Obvious differences could be found in area a. However, in Los Angeles both the maximum subsidence (97.6 mm) and uplift (117.2 mm) are smaller after correction (see Fig. 6).

Please cite this article in press as: M. Lei, et al., Influence of ocean tidal loading on InSAR offshore areas deformation monitoring, Geodesy and Geodynamics (2017), http://dx.doi.org/10.1016/j.geog.2016.09.004

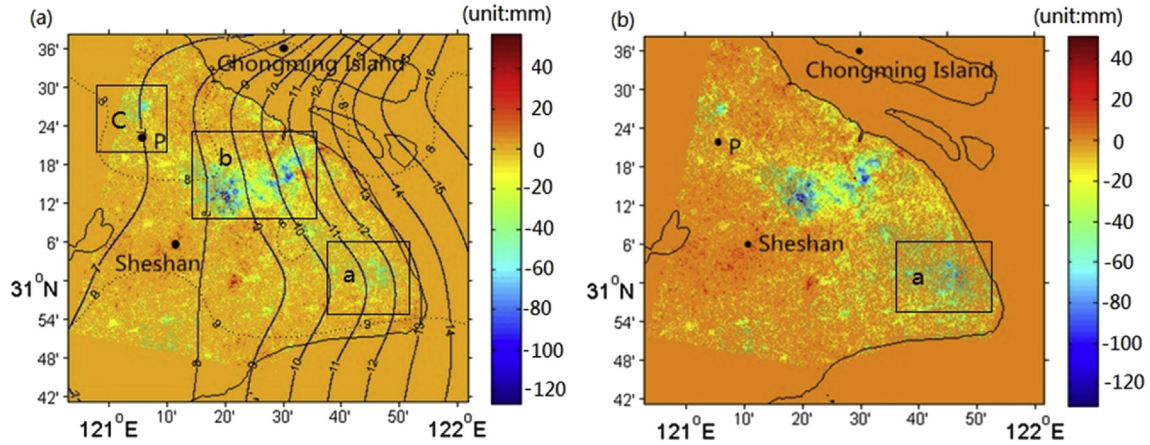

Fig. 5. (a) InSAR deformation and *M*2 tidal constituent distribution in Shanghai; (b) InSAR deformation corrected by *M*2 tidal constituent in Shanghai. The black solid lines show the coastline. The blue contour line represents the OTL displacement in the vertical direction; the black dashed lines show the atmospheric loading in the vertical direction. Both of them are positive on the upward. Areas a, b and c have remarkable subsidence.

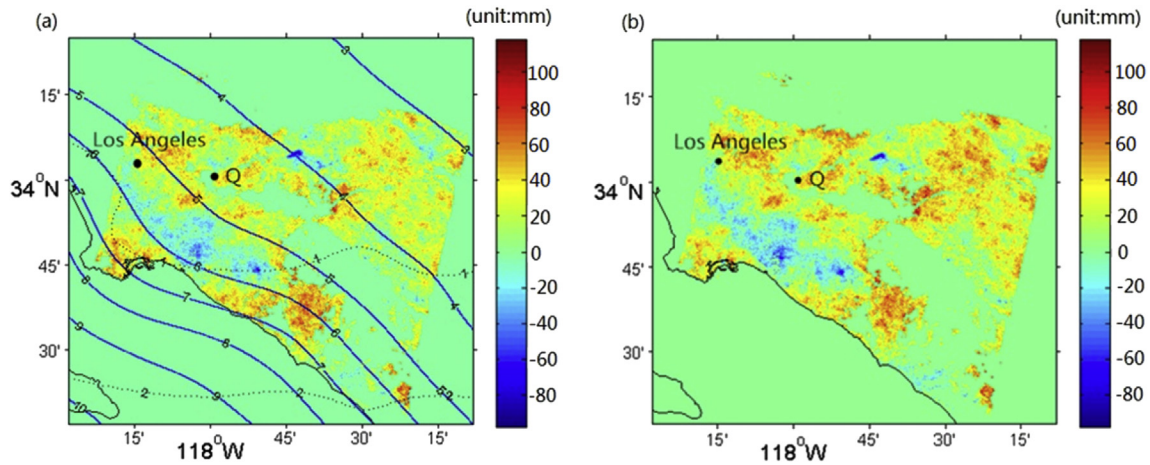

Fig. 6. (a) InSAR deformation data and *M*2 tidal constituent distribution in Los Angeles; (b) InSAR deformation corrected with *M*2 OTL in Los Angeles. The blue contour lines represent the OTL displacement in the vertical direction, the red dashed lines show the atmospheric loading in the vertical direction. Both of them are positive on the upward.

To assess the effects of the corrected InSAR, we used IGS stations within the framework of the ITRF2005 provided by the International Terrestrial Reference Frame (ITRF) as reference points. We choose Sheshan IGS site in Shanghai and nine IGS sites in Los Angeles for the comparative analysis. Then we obtain the LOS displacement relative to point P from 1992 to 2000 in Sheshan, and the LOS displacement relative to point Q from 2005 to 2010 in Los Angeles. Then we compute the accuracy achievement by the following formula.

Table 4
—InSAR deformation with and without OTL corrections and deformation obtained by IGS stations.

IGS sites	GPS monitoring	InSAR (mm) (with corrections)	InSAR (mm) (without corrections)	Percentage error (%)
SHAO	10.7	13.6	16.1	15.5
GHRP	54.1	49.6	42.1	17.8
LBC1	−31.3	−31.3	−25.4	23.2
LBC2	42.5	40.5	48.2	16
LBCH	44.5	46.9	55.3	15.2
LGWD	31	34.8	42.8	18.7
RTHS	56.1	54.9	48.4	13.4
SGHS	48.9	49.3	49.8	1
TWMS	35.9	34.9	33.4	4.5
P471	8	8.5	13.5	37

$$percentage\ error = \left|\frac{D_{after} - D_{before}}{D_{before}}\right| \times 100\% \quad (8)$$

where D_{after} and D_{before} are the InSAR deformation with and without OTL corrections, respectively.

As Table 4 shows, the corrected InSAR deformation is closer to that of IGS sites. The accuracy improvements at most sites (except for SGHS and TWMS) are fairly good, especially at P471 (37%) and the Sheshan station (15.5%). Also, the smaller the deformation, the better the correcting effect. As a result, when we use InSAR to detect smaller displacement, the OTL should be considered.

5. Conclusion

In this study, we improved regional ocean tide model by assimilating data from 60 offshore gauge stations in China (55 gauge stations in the South China Sea and 5 gauge stations in the Bohai Sea), Then compared its precision with other models using the *M*2 and *K*1 tidal components. The results show that the improved regional model has much higher accuracy than the TPXO7.2-ATLAS model, especially in the South China Sea. Compared with the osu.chinasea.2010 model, the improved

Please cite this article in press as: M. Lei, et al., Influence of ocean tidal loading on InSAR offshore areas deformation monitoring, Geodesy and Geodynamics (2017), http://dx.doi.org/10.1016/j.geog.2016.09.004

regional model shows no obvious improvement in effectiveness, which may be caused by insufficient assimilation data. In order to improve the precision of OTL displacement in some sites of China, we use the improved regional model to replace the offshore part of the global model to generate the present model, which is then be used to calculate the amplitude and phase lag of *M*2, *K*1 tidal constituent of 17 IGS stations in China. The observations of FES2004, TPXO7.2-ATLAS, NAO99JB are used for reference. The results show that both diurnal tides and semi-diurnal tides have great influence on precise positioning and small deformation detection. The OTL displacement of coastal sites calculated by the present model is 2–3 mm larger than other models. For the rest regions the difference among these models is less than 1 mm. It turned out that the present model can effectively increase the precision of OTL displacement correction in coastal areas.

We applied the present model to InSAR deformation monitoring in Shanghai and Los Angeles, and compare the results with the IGS displacements. The comparison demonstrates that the accuracy of InSAR deformation can be improved by about 20% with OTL correction, and the maximum improvement is 37%. What's more, the smaller the deformation is, the greater the improvement. Therefore, when we use InSAR to detect small displacement, the OTL should be considered. This work enriches the OTL displacement correction on coastal deformation monitoring using InSAR.

Acknowledgments

The authors thank Duncan Agnew for providing the SPOTL software. We also thank European Space Agency (ESA) for providing us with ERS-1/2 SAR data. This work is supported by the National Natural Science Foundation of China (41404013, U1531128).

References

[1] N.T. Penna, M.S. Bos, T.F. Baker, H.G. Scherneck, Assessing the accuracy of predicted ocean tide loading displacement values, J. Geod. 82 (12) (2008) 893–907.
[2] S.N. Madsen, H.A. Zebker, J. Martin, Topographic mapping using radar interferometry: processing techniques, IEEE T. Geosci. Remote 31 (1) (1993) 246–256.
[3] E.W. Schwiderski, On charting global ocean tides, Rev. Geophys. 18 (1) (1980) 243–268.
[4] D. Massonnet, M. Rossi, C. Carmona, F. Adragna, G. Peltzer, Feiglk, et al., The displacement field of the Landers earthquake mapped by radar interferometry, Nature 364 (1993) 138–142.
[5] L. Padman, S. Erofeeva, I. Joughin, Tides of the ross sea and ross ice shelf cavity, Antarct. Sci. 15 (15) (2003) 31–40.
[6] Zhiwei Li, Zefa Yang, Jianjun Zhu, Jun Hu, Yunjia Wang, Peixian Li, et al., Retrieving three-dimensional displacement fields of mining areas from a single InSAR pair, J. Geod. 89 (1) (2015) 17–32.
[7] Jia Li, Zhiwei Li, Xiaoli Ding, Qijie Wang, Jianjun Zhu, Changcheng Wang, Investigating mountain glacier motion with the method of SAR intensity-Tracking: removal of topographic effects and analysis of the dynamic patterns, Earth Sci. Rev. 138 (2014) 179–195.
[8] J. Hu, Q.J. Wang, Z.W. Li, R.A. Xie, X.Q. Zhang, Q. Sun, Retrieving three-dimensional coseismic displacements of the 2008 Gaize, Tibet earthquake from multi-path interferometric phase analysis, Nat. Hazards 73 (3) (2014) 1311–1322.
[9] Shanshan Li, Zhiwei Li, Jun Hu, Qian Sun, Xiaoying Yu, Investigation of the seasonal oscillation of the permafrost over Qinghai-Tibet plateau with SBAS-InSAR algorithm, Chin. J. Geophys. 56 (5) (2013) 1476–1486.
[10] S.R. Cloude, K.P. Papathanassiou, Three-stage inversion process for polarimetric SAR interferometry, IEE P.-Radar Son. Nav. 150 (3) (2003) 125–134.
[11] R.M. Goldstein, H. Engelhardt, B. Kamb, R.M. Frolich, Satellite radar interferometry for monitoring ice sheet motion: application to an Antarctic ice stream, Science 262 (5139) (1994) 1525–1530.
[12] Melachroinos, A. Stavros, R. Biancale, M. Llubes, F. Perosanz, M. Lyard, et al., Ocean tide loading (OTL) displacements from global and local grids: comparisons to GPS estimates over the shelf of Brittany, France, J. Geod. 82 (6) (2008) 357–371.
[13] Christopher J. DiCaprio, Mark Simons, Importance of ocean tidal load corrections for differential InSAR, Geophys. Res. Lett. 35 (22) (2008) 91–96.
[14] E. Rignot, L. Padman, D.R. MacAyeal, M. Schmeltz, Observation of ocean tides below the Filchner and Ronne Ice Shelves, Antarctica, using synthetic aperture radar interferometry: comparison with tide model predictions, J. Geophys. Res. 105 (8) (2000) 19615–19630.
[15] W.E. Farrell, Deformation of the earth by surface loads, Rev. Geophys. 10 (3) (1972) 761–797.
[16] GuoHong Fang, XiaoQing Xu, Zexun Wei, Yonggang Wang, Xinyi Wang, Vertical displacement loading tides and self-attraction and loading tides in the Bohai, Yellow, and East China Seas, Sci. China Earth Sci. 56 (2013) 63–70.
[17] C. Hwang, J.F. Huang, Sgotl: a computer program for modeling high-resolution, height-dependent gravity effect of ocean tide loading, Terr. Atmos. Ocean. Sci. 23 (2) (2012) 219–229.
[18] G. Blewitt, GPS and space-based geodetic methods, in: Tom Herring (Ed.), Geodesy: treatise on geophysics, Elsevier, Holland, 2007, pp. 307–338.
[19] C. Wunsch, D. Stammer, Atmospheric loading and the oceanic "inverted barometer" effect, Rev. Geophys. 35 (1) (1997) 79–107.
[20] J.P. Boy, J. Hinderer, P. Gegout, Global atmospheric loading and gravity, Phys. Earth Planet. In. 109 (3) (1998) 161–177.
[21] T. Mayer-Gurr, R. Savcenko, W. Bosch, I. Daras, F. Flechtner, DahleC. Ocean tides from satellite altimetry and grace, J. Geodyn. 60 (16) (2012) 28–38.
[22] K. Matsumoto, T. Takanezawa, M. Ooe, Ocean tide models developed by assimilating TOPEX/POSEIDON altimeter data into hydrodynamical model: aglobal model and a regional model around Japan, J. Oceanogr. 56 (5) (2000) 567–581.
[23] D. Stammer, R.D. Ray, O.B. Andersen, B.K. Arbic, W. Bosch, L. Carrere, et al., Accuracy assessment of global barotropic ocean tide models, Rev. Geophys. 52 (3) (2014) 243–282.

Mengfei Lei, is a postgraduate in Central South University. His study interests include the geodesy and geodynamic. His main research orientations is ocean tide models and ocean tide loading.

Please cite this article in press as: M. Lei, et al., Influence of ocean tidal loading on InSAR offshore areas deformation monitoring, Geodesy and Geodynamics (2017), http://dx.doi.org/10.1016/j.geog.2016.09.004